THE JOURNAL OF BIOLOGICAL CHEMISTRY VOL. 291, NO. 19, pp. 9960–9973, May 6, 2016
Published in the U.S.A.

Structural Studies of *Medicago truncatula* Histidinol Phosphate Phosphatase from Inositol Monophosphatase Superfamily Reveal Details of Penultimate Step of Histidine Biosynthesis in Plants*[S]

Received for publication, December 6, 2015, and in revised form, March 11, 2016 Published, JBC Papers in Press, March 18, 2016, DOI 10.1074/jbc.M115.708727

Milosz Ruszkowski[1] **and Zbigniew Dauter**

From the Synchrotron Radiation Research Section of MCL, NCI, National Institutes of Health, Argonne, Illinois 60439

The penultimate enzyme in the histidine biosynthetic pathway catalyzes dephosphorylation of L-histidinol 1-phosphate (HOLP) into L-histidinol. The recently discovered in *Arabidopsis thaliana* plant-type histidinol phosphate phosphatase (HPP) shares no homology with the two other HPP superfamilies known previously in prokaryotes and resembles *myo*-inositol monophosphatases (IMPases). In this work, identification of an HPP enzyme from a model legume, *Medicago truncatula* (*Mt*HPP) was based on the highest sequence identity to *A. thaliana* enzyme. Biochemical assays confirmed that *Mt*HPP was able to cleave inorganic phosphate from HOLP but not from D-*myo*-inositol-1-phosphate, the main substrate of IMPases. Dimers of *Mt*HPP, determined by size exclusion chromatography, in the presence of CO_2 or formaldehyde form mutual, methylene-bridged cross-links between Lys^{158} and Cys^{245} residues. Four high resolution crystal structures, namely complexes with HOLP (substrate), L-histidinol (product), and PO_4^{3-} (by-product) as well as the structure showing the cross-linking between two *Mt*HPP molecules, provide detailed structural information on the enzyme. Based on the crystal structures, the enzymatic reaction mechanism of IMPases is accustomed to fit the data for *Mt*HPP. The enzymatic reaction, which requires Mg^{2+} cations, is catalyzed mainly by amino acid residues from the N-terminal domain. The C-terminal domain, sharing little identity with IMPases, is responsible for the substrate specificity (*i.e.* allows the enzyme to distinguish between HOLP and D-*myo*-inositol-1-phosphate). Structural features, mainly the presence of a conserved Asp^{246}, allow *Mt*HPP to bind HOLP specifically.

L-Histidine (His) is one of the 20 standard, proteinogenic amino acids, vital for any living organism. The side chain of His, the imidazole moiety, can be protonated at Nδ and/or Nϵ. Given the very high pK_a of 14.5 (1), it is very unlikely that doubly deprotonated His exists in proteins. The role of His in proteins is related to its ability to switch protonation states within the range of physiological conditions. His is present in active sites of many enzymes, where it coordinates zinc, nickel, or other metal cations. Also, free, unincorporated into proteins His has been reported to chelate nickel ions in plant species that hyperaccumulate this metal (2, 3). In bacteria, fungi, and plants, His phosphorylation is a ubiquitous mechanism, used in two-component signal transduction (4). To humans, His is one of nine essential amino acids; thus, unraveling the details of its biosynthesis in plants is of particular interest (5).

His is also one of the least abundant amino acids in proteins, probably because its biosynthesis is metabolically expensive (6), with 31–41 ATP molecules required to produce a single His molecule (7–9). Plants biosynthesize His similarly to prokaryotes (10). The 11-step pathway, which originates from 5′-phosphoribosyl 1-pyrophosphate, is catalyzed by eight enzymes, HISN1–8, three of which (HISN2, -4, and -8) are bifunctional. His biosynthesis is connected to tryptophan (11) and nucleotide (7, 11) metabolic pathways. Also, during the course of His production, two other amino acids, glutamic acid and glutamine, serve as nitrogen donors.

Unlike for many other amino acids, most of the enzymes from the His biosynthetic pathway are encoded by single genes (12), and, because the His biosynthetic pathway is absent in animals, plant enzymes involved in His production could potentially serve as targets in the search for herbicides. Of the eight enzymes required for His biosynthesis in plants, seven were identified in the last decades of the twentieth century: HISN1 (13), HISN2 (14), HISN3 (15), HISN4 (16), HISN5 (13), HISN6 (17), and HISN8 (18–20). Although HISN7 activity *in planta* was reported in 1971 (13), it was unknown which particular protein was responsible for this action. HISN7 catalyzes dephosphorylation of L-histidinol 1-phosphate (HOLP)[2] to L-histidinol (HOL) (Fig. 1); therefore, a HISN7 enzyme is a histidinol phosphate phosphatase (HPP) (EC 3.1.3.15).

For a long time, it was thought that bacterial HPP enzymes belonged to either of the two superfamilies: (i) containing conserved Asp residues (DDDD) (21, 22) or (ii) polymerase and

* This project was supported in part by the Intramural Research Program of the NCI, National Institutes of Health, Center for Cancer Research. The authors declare that they have no conflicts of interest with the contents of this article. The content is solely the responsibility of the authors and does not necessarily represent the official views of the National Institutes of Health.

[S] This article contains supplemental material.

The atomic coordinates and structure factors (codes 5EQ7, 5EQ8, 5EQ9, and 5EQA) have been deposited in the Protein Data Bank (http://wwpdb.org/).

[1] To whom correspondence should be addressed: Synchrotron Radiation Research Section, MCL, National Cancer Institute, S. Cass Ave. 9700, Bldg. 202, Rm. Q-141, Argonne, IL 60439. E-mail: mruszkowski@anl.gov.

[2] The abbreviations used are: HOLP, L-histidinol 1-phosphate; HOL, L-histidinol; HPP, histidinol phosphate phosphatase; PHP, polymerase and histidinol phosphatase(s); IMPase, *myo*-inositol monophosphatase; IMP, D-*myo*-inositol-1-phosphate; TCEP, tris(2-carboxyethyl)phosphine; BisTris, 2-[bis(2-hydroxyethyl)amino]-2-(hydroxymethyl)propane-1,3-diol.

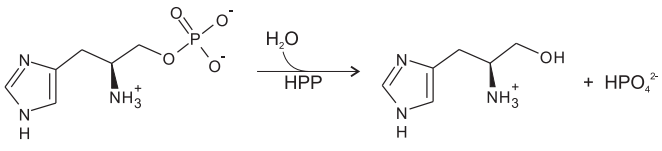

FIGURE 1. **Scheme of the enzymatic reaction catalyzed by HPP enzymes.**

histidinol phosphatases (PHP) (23). It was therefore confusing that plant genomes did not contain sequences coding for HPP proteins from either DDDD or PHP superfamilies. When a third superfamily of HPP enzymes was discovered in *Corynebacterium glutamicum* (24) and *Streptomyces coelicolor* (25), it shed new light on the missing link of His biosynthesis. Sequences of the enzymes from the novel HPP superfamily showed significant similarity to *myo*-inositol monophosphatases (IMPases). In *Arabidopsis thaliana*, three IMPase or IMPase-like proteins were identified and reported: VTC4, IMPL1 (IMPase-like 1), and IMPL2 (IMPase-like 2) (26). Of those three candidates, only *At*IMPL2 was shown to possess HPP activity (27). Moreover, although *At*IMPL2 was still able to dephosphorylate, for example, D-*myo*-inositol-1-phosphate (IMP) (26), HPP activity was proposed to be the only reaction catalyzed *in vivo* by this enzyme (28). It is also worth mentioning that the growth of *Atimpl2* mutants was severely compromised but was rescued by external supplementation with His (28). Similarly to other proteins involved in His biosynthesis, *At*IMPL2 contains chloroplast-targeting signal peptide and has been actually localized in chloroplasts (27).

To date, *At*IMPL2 has been the only identified plant HPP enzyme. Here we report the identification of a second member of the plant-type superfamily of HPP enzymes and its thorough structural characterization (*i.e.* the first structure of IMPase-like HPP enzyme from any domain of life). These studies were performed on *Medicago truncatula*, a model legume plant, and the target enzyme is referred to as *Mt*HPP. Four high resolution crystal structures (complexes with PO_4^{3-}, HOLP, and HOL and a structure illustrating a unique cross-linking interaction between two *Mt*HPP molecules) are described within the scope of this research. Presented results illustrate the exact mode of HOLP binding (*i.e.* which residues interact with the substrate) as well as clarify the requirements for Mg^{2+} ions. The structures also indicate important differences in the reaction mechanism between IMPases and *Mt*HPP. Moreover, the structural features, which allow *Mt*HPP to bind HOLP, are compared with the IMP binding site of a classic IMPase to explain why IMPases are unable to bind HOLP. *Mt*HPP, as a member of the novel, third superfamily of HPP enzymes, shares little to no similarity with the previously described HPPs from the DDDD and PHP superfamilies. Therefore, the presented work provides new, important details of His biosynthesis in plants. The results can also be extrapolated to those bacterial species that rely on IMPase-like HPPs.

Experimental Procedures

Cloning, Overexpression, and Purification of MtHPP—The total RNA was isolated from *M. truncatula* roots using the RNeasy plant minikit (Qiagen). SuperScript II reverse transcriptase (Life Technologies) with oligo(dT) (15 and 18) primers was utilized to obtain the coding DNA (cDNA). The cDNA served as a template for acquiring the sequence coding for the *Mt*HPP open reading frame by polymerase chain reaction (PCR). The used primers (forward, TACTTCCAATCCAATGCCATGTCCTCCTCATCTTCGCCTC; reverse, TTATCCACTTCCAATGTTACTACCATTGTAATGAATCTAGAGCCTGTT) allowed the use of a ligase-independent cloning method (29) for incorporating the insert into pMCSG68 vector (Midwest Center for Structural Genomics). The pMCSG68 vector introduces a His_6 tag followed by the tobacco etch virus protease cleavage site at the N terminus of the expressed protein. The final polypeptide carries an SNA N-terminal fragment before the genuine protein sequence. The correctness of the insert was confirmed by DNA sequencing.

Overexpression was carried out in BL21 Gold *Escherichia coli* cells (Agilent Technologies). The bacteria were cultured with shaking at 210 rpm in LB medium supplemented with 150 μg/ml ampicillin at 37 °C until the A_{600} reached 1.0. The cultures were cooled down to 18 °C, and *Mt*HPP production was induced by the addition of isopropyl-D-thiogalactopyranoside at a final concentration of 0.5 mM. The culture was grown for 18 h and then centrifuged at 3500 × *g* for 20 min at 4 °C. Cell pellet from 1 liter of culture was resuspended in 35 ml of binding buffer (50 mM Tris-HCl, pH 8.0, 500 mM NaCl, 20 mM imidazole, 1 mM tris(2-carboxyethyl)phosphine (TCEP)) and stored at −80 °C. The samples were thawed, and the cells were disrupted by sonication using bursts of total duration of 4 min, with appropriate intervals for cooling. Cell debris was pelleted by centrifugation at 25,000 × *g* for 30 min at 4 °C. The supernatant was applied to a column packed with 6 ml of HisTrap HP resin (GE Healthcare), connected to a VacMan manifold (Promega), and the chromatographic process was accelerated with a vacuum pump. After binding, the column was washed five times with 40 ml of the binding buffer, and His_6-tagged *Mt*HPP was eluted with 20 ml of elution buffer (50 mM Tris-HCl, pH 8.0, 500 mM NaCl, 300 mM imidazole, 1 mM TCEP). The His_6 tag was cleaved with tobacco etch virus protease (final concentration 0.1 mg/ml), and the excess of imidazole was removed by dialysis (overnight at 4 °C) simultaneously. The solution was mixed with HisTrap HP resin to eliminate the cleaved His_6 tag and the His_6-tagged tobacco etch virus protease. The flow-through was collected, concentrated to 4 ml, and applied on a HiLoad Superdex 200 16/60 column (GE Healthcare) equilibrated with a buffer composed of 25 mM Tris-HCl, pH 8.0, 200 mM NaCl, and 1 mM TCEP.

Generation of Site-directed Mutants—Site-directed mutagenesis of *Mt*HPP was performed using a polymerase incomplete primer extension technique (30). The plasmid isolated from bacterial strain used for the overexpression of the wild-type *Mt*HPP served as a template. A T151A mutation (underlined) was introduced using two primers: GGA<u>GCT</u>AAGAGCTTTATCACTGGGAAAC (coding strand) and TCTT<u>AGC</u>TCCATCAATAGGATCTAATACCC (complementary strand). The ^{245}CDC^{247} to ^{245}AAA^{247} mutant (*Mt*HPP-AAA) was generated using primers GGT<u>GCTGCCGCA</u>TATGCATATGCTC and ATA<u>TGCGGCAGC</u>ACCATATAATGGAATTTTAAC. The sequences of resulting plasmids were verified by

DNA sequencing. Both mutated proteins were overexpressed and purified according to the protocol developed for the wild-type enzyme.

Crystallization and Data Collection—*Mt*HPP was concentrated using Amicon concentrators (Millipore) to 19 mg/ml as determined by measuring the absorbance at 280 nm with an extinction coefficient of 46,400. Crystallization screening was performed using a robotic sitting drop vapor diffusion setup (Mosquito). The most promising hits were optimized manually in a hanging drop configuration. Crystals of *Mt*HPP complex with free phosphate grew in 15% PEG 3350, 0.2 M diammonium hydrogen phosphate, pH 8.0. Paraton-N suited as a cryoprotectant. Aiming at the HOLP complex, crystals from the same condition were washed in a crystallization solution supplemented with 2 mM $MgCl_2$, 5 mM HOLP, and 20% glycerol and were immediately vitrified in liquid nitrogen. Crystals grown in 30% PEG 3350, 0.1 M BisTris, pH 6.5, 0.2 M ammonium acetate, 10 mM magnesium acetate were incubated (i) for 8 min with 5 mM HOLP and flash-frozen in Paraton-N to obtain structure with HOL or (ii) overnight over the reservoir supplemented with 100 mM formaldehyde to complete cross-linking between Lys^{158} and Cys^{245} and vitrified in Paraton-N. Diffraction data were collected at 22-ID (complexes with PO_4^{3-} or HOL and cross-linked) and 19-ID (HOLP complex) beamlines at the Advanced Photon Source (Argonne, IL). The diffraction images were processed with *XDS* (31). Statistics of the data collection and processing are summarized in Table 1.

Determination and Refinement of the Crystal Structures—The crystal structure of *Mt*HPP was solved by molecular replacement with *PHASER* (32), using the closest homolog for which the crystal structure was available, IMPase from *Zymomonas mobilis*, as the search probe (33) (Protein Data Bank (PDB) entry 4N81, 45% sequence identity). Automatic model building was carried out with the on-line version of *ARP/wARP* (34). The atomic coordinates were placed inside the unit cell with *ACHESYM* server (35). *COOT* (36) was used for manual fitting in the electron density maps between rounds of model refinement in Refmac (37). Riding hydrogen atoms for the protein chain were included in the refinement with anisotropic atomic displacement parameters. The refinement statistics are listed in Table 1.

Determination of the Oligomeric State in Solution—The *Mt*HPP elution profile from size exclusion chromatography was tested against gel filtration standard (1511901, Bio-Rad). Two independent experiments were performed: (i) injection of 3 ml of *Mt*HPP and standard samples onto a HiLoad Superdex 200 16/60 column (GE Healthcare) at a flow rate of 1 ml/min and (ii) injection of 100-μl samples onto a Superdex 200 10/300 GL column (GE Healthcare) at a flow rate of 0.5 ml/min.

Cross-linking in the presence of formaldehyde vapors or carbon dioxide atmosphere was tested using *Mt*HPP at a 0.5 mg/ml concentration, dissolved in buffer composed of 25 mM HEPES, pH 8.0, 50 mM NaCl, with or without 1 mM TCEP. An experiment with formaldehyde cross-linking was performed over 24 h by placing an open vial with 300 μl of protein solution above a thin layer of formaldehyde (36% solution) in a closed bottle. To test the covalent dimer formation in the presence of CO_2 in a separate experiment, the open vials with protein solutions were positioned in a bottle connected (with rubber hosing) to a Styrofoam box with dry ice. The flow of gaseous CO_2 to the chamber containing vials with protein was tested daily by quenching flame from a lighter, and the dry ice was replenished when needed.

Mass Spectrometry—The samples were run through an Agilent 1290 liquid chromatograph with acetonitrile/water/acetic acid solvent on a Poroshell C3 reverse phase column onto an Agilent 6130 quadrupole mass spectrometer. For each sample, 3 μl was loaded with a protein concentration of ~0.5 mg/ml, dissolved in 25 mM HEPES, pH 8.0, and 50 mM NaCl. Results were analyzed using the Agilent Chemstation software. For details, see the supplemental material.

Enzymatic Tests—The physiological, forward reaction of *Mt*HPP was measured at room temperature. The phosphatase activity was determined by measuring the concentration of inorganic phosphate by an improved malachite green assay (38). Reactions were carried out in 200-μl volumes in a buffer containing 20 mM Tris-HCl, pH 8.0, 50 mM NaCl, 2 mM $MgCl_2$. Seven concentrations of the substrate (HOLP xLi, catalog no. 41486, Sigma) were used: 50, 100, 200, 400, 600, 800, and 1000 μM. Prior tests confirmed that within this range of concentrations, the rate of the reaction is linear for >4 min. Enzymatic reactions were initiated by the addition of *Mt*HPP to a final concentration of 20 nM and, after 4 min, quenched with 200 μl of the color reagent. The samples were diluted with 600 μl of H_2O to a final volume of 1 ml. Standard reactions to evaluate optimal pH, Mg^{2+} concentration, and Li^+ inhibition were carried out using 50 μM HOLP to minimize the carryover of Li^+ cations from HOLP × lithium salt. Activity of *Mt*HPP-T151A and *Mt*HPP-AAA mutants *versus* wild-type *Mt*HPP was evaluated using 200 μM HOLP or 200 μM IMP (catalog no. 10007777, Cayman Chemicals). To ensure lack of measurable activity of both mutants, the mixture was let react for 10 min in a separate set of experiments. All assays were performed in triplicate. Absorbance was measured at 630 nm using a PharmaSpec UV-1700 spectrophotometer (Shimadzu). The amount of free phosphate was calculated on the assumption of a molar extinction coefficient for malachite green-phosphomolybdate complex of 90,000 M^{-1} cm^{-1}. Non-linear regression analysis was computed with Prism version 6.07 (GraphPad Software).

Other Software Used—Molecular figures were created with UCSF *Chimera* (39). Root mean square deviations were calculated in the same program. Ramachandran plot was calculated in *Rampage* (40). Structural features were recognized with ProMotif (41) within the PDBsum server (42). A phylogenetic tree of proteins containing the identical, 11-amino acid sequence motif based on a PSI-BLAST search (43) was constructed in MEGA6 (44). Signal peptides were recognized using the TargetP version 1.1 server (45, 46).

Results and Discussion

Identification of the Histidinol Phosphate Phosphatase in M. truncatula—To identify the HPP enzyme in *M. truncatula*, the BLAST server (47) was applied. *At*IMPL2 protein sequence (UniProt accession number Q6NPM8) (27, 28), without the signal peptide, was used as the search probe. The three homologs in *M. truncatula* proteome (48), with the highest identity to

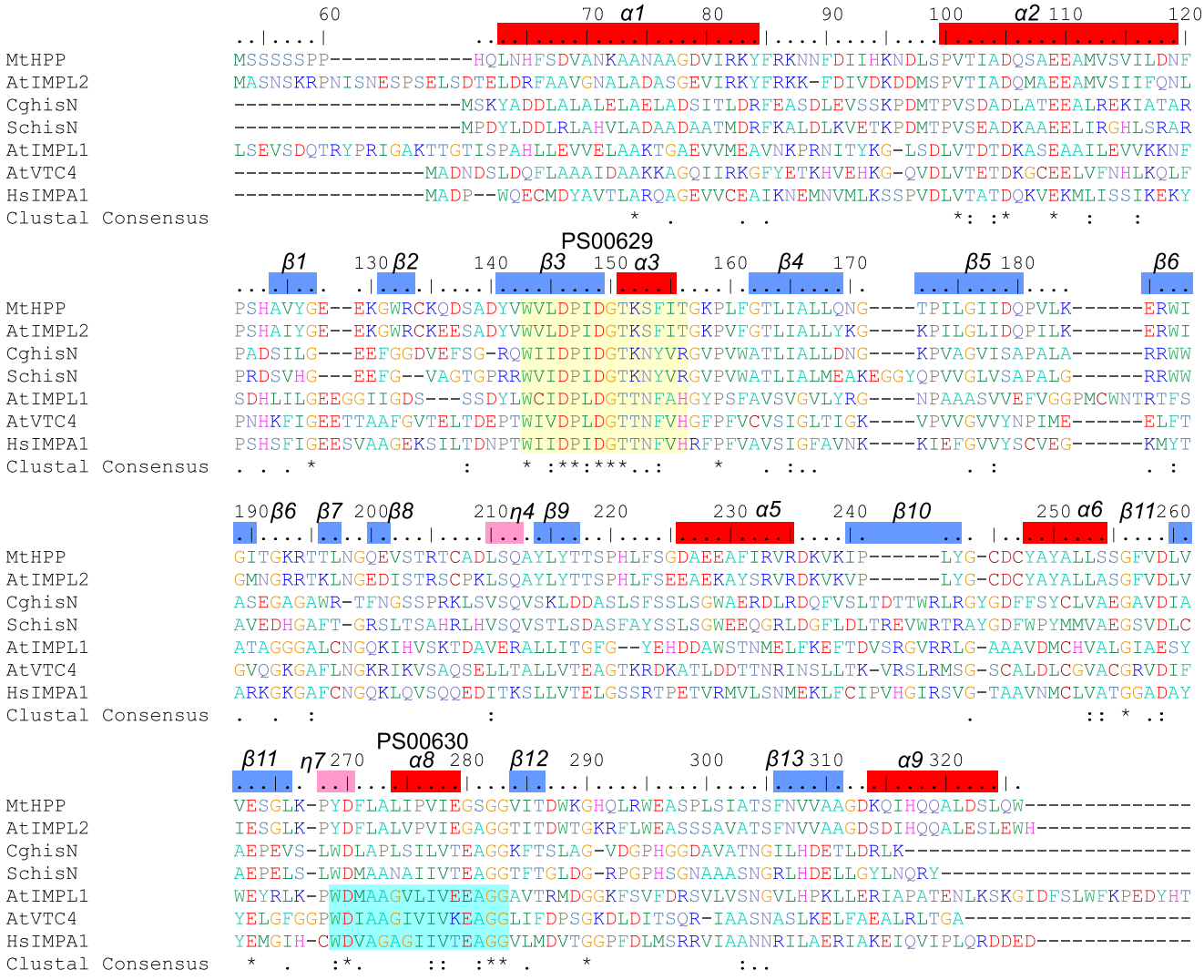

FIGURE 2. **Sequence alignment.** *Numbering* of the residues corresponds to the *Mt*HPP sequence. UniProt accession numbers are given in parentheses: *Mt*HPP (G7J7Q5) cleaved at position 52; *At*IMPL2 (Q6NPM8) cleaved at 61; *C. glutamicum* hisN (Q8NS80); *S. coelicolor* hisN (Q9K4B1); *At*IMPL1 (Q94F00) cleaved at 61 and without 2 C-terminal residues; *At*VTC4 (Q9M8S8); *Hs*IMPA1 (P29218). *Bars above* the sequence illustrate secondary structure elements based on *Mt*HPP-PO_4^{3-} complex: α helices (*red*), 3_{10} helices (*pink*), and β strands (*blue*). *Pale yellow shading* indicates PROSITE pattern PS00629, whereas *light blue* marks PS00630.

*At*IMPL2, all annotated as IMPases, were located in the same locus in the genome (Medtr3g117220), which indicated either three splicing forms of the enzyme or artifacts of *in silico* prediction. The form with highest identity and query cover to the *Arabidopsis* enzyme, of 75 and 92%, respectively (UniProt accession number G7J7Q5) was therefore chosen as the target protein (Fig. 2). The N-terminal signal peptide, which *in vivo* targets *Mt*HPP to chloroplast, was determined by the TargetP version 1.1 server (45, 46). The cleavage was predicted to occur between Arg^{51} and Ala^{52}, and the overexpressed construct was designed to yield the final protein with sequence starting from Met^{53}.

Enzymatic tests revealed that indeed, in the presence of Mg^{2+}, *Mt*HPP was able to hydrolyze HOLP to HOL, with the release of inorganic phosphate. The optimal Mg^{2+} concentration and pH for the enzyme was determined to be 5 mM and 8.4, respectively. However, for enzymatic tests, these values were lower, to reflect conditions in illuminated (daytime) chloroplast stroma, namely 2 mM Mg^{2+} (49) and pH 8.0 (50, 51).

Because enzymes from the IMPase family are inhibited by Li^+ cations (52–54), and HOLP is commercially available only as lithium salt, *Mt*HPP activity was tested against increasing Li^+ concentration. Up to 1 mM Li^+, which reflects the milieu with 1 mM HOLP on the assumption of complete dissociation of HOLP × lithium salt, the enzyme retained 83% of its initial activity. The estimated half-inhibition dose, $IC_{50} \approx 5.5$ mM Li^+, means that *Mt*HPP is much less susceptible to Li^+ inhibition than *At*IMPL2 ($IC_{50} \approx 1.5$ mM (28)) and bovine *myo*-inositol-1-phosphatase ($IC_{50} \approx 0.8$ mM (54)) and more similar in this behavior to *At*VTC4 ($IC_{50} \approx 3.5$–5 mM (26)).

The obtained Michaelis-Menten constant (K_m) of *Mt*HPP for HOLP hydrolysis of 263 ± 28 μM (Fig. 3) is between 180 and 400 μM reported for the *Arabidopsis* (28) and wheat (13) enzymes, respectively. On the other hand, *Mt*HPP catalyzes the reaction at a higher rate than *At*IMPL2 because the two catalytic constants (k_{cat}) are 3.6 ± 0.14 and 1.3 ± 0.2 s^{-1}, respectively. Altogether, the catalytic efficiency (k_{cat}/K_m) calculated for *Mt*HPP ($13.7 \pm 1.9 \times 10^3$) exceeds the value reported for *At*IMPL2

($7.9 \pm 0.2 \times 10^3$ (28)). On the other hand, neither *Mt*HPP nor *Mt*HPP-T151A or *Mt*HPP-AAA mutants have shown any detectable activity against IMP, which confirms previous observations that IMPase-like HPPs play a role only in His biosynthesis (28).

Overall Structure of MtHPP—The structures of *Mt*HPP complexes were solved and refined using x-ray diffraction data ranging to high resolution (Table 1). The obtained electron density maps allowed us to trace without ambiguity almost the entire protein chain. The exceptions are 9 ± 1 (chain- and complex-dependent) N-terminal amino acids and the mobile loop between helices α1 and α2.

A monomer of *Mt*HPP has an αβαβα sandwich-like arrangement (Fig. 4). The N-terminal domain, which forms an α + β structure, covers residues from the N terminus to Glu^{201}. Two long α-helices (α1 and α2) are separated by a mobile loop that is

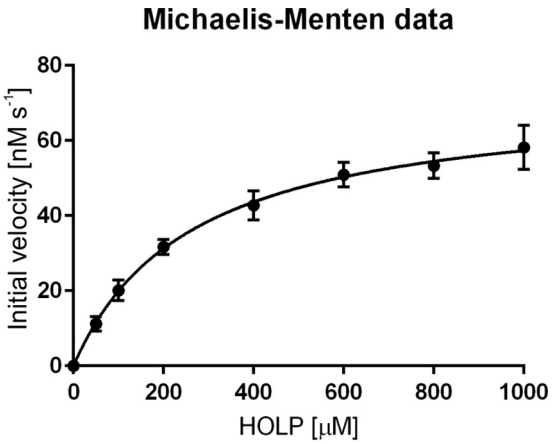

FIGURE 3. **Kinetic analysis of *Mt*HPP activity with HOLP.** The measurements were fit to a non-linear curve in Prism version 6.07 software (GraphPad), based on the Michaelis-Menten equation, to calculate K_m and k_{cat}. *Error bars*, S.D. calculated from three independent replications.

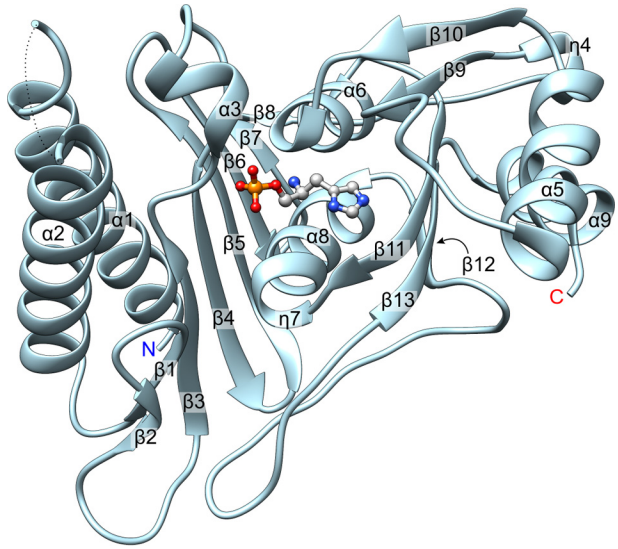

FIGURE 4. **Overall structure of *Mt*HPP monomer with secondary structure elements.** Chain A from *Mt*HPP in complex with HOLP (*ball-and-stick representation*) is shown. The *black dotted line* represents the mobile loop absent in the electron density. Termini are denoted as *blue* (*N*) and *red* (*C*) *letters*. The *numbering* of α- and η (3_{10})-helices is consecutive, regardless of the twist of the helix.

TABLE 1

Data collection and refinement statistics

Values in parentheses correspond to the highest resolution shell.

	PO_4^{3-}	HOL	HOLP, Mg^{2+}	Lys-CH_2-Cys
Data collection				
Wavelength (Å)	0.9920	0.7999	0.9793	0.7999
Space group	$P42_12$	$P42_12$	$P2_1$	$P2_1$
Unit cell parameters				
a, *b*, *c* (Å)	87.0, 87.0, 61.9	87.3, 87.3, 61.8	61.9, 89.8, 92.6	62.2, 89.4, 92.2
α, β, γ (degrees)	90, 90, 90	90, 90, 90	90, 97.1, 90	90, 96.9, 90
Oscillation range (degrees)	0.5	0.5	0.5	0.5
No. of images	720[a]	400	500	400[a]
Resolution (Å)	40–1.19 (1.22–1.19)	40–1.30 (1.38–1.30)	40–1.36 (1.44–1.36)	40–1.32 (1.35–1.32)
Reflections collected/unique	2,617,572/76,240	951,848/59,314	1,102,015/214,644	1,204,836/234,185
Completeness (%)	99.9 (99.1)	99.6 (97.8)	99.8 (98.8)	99.9 (99.9)
Multiplicity	34.3 (5.5)	16.0 (15.4)	5.1 (5.0)	5.1 (4.2)
R_{meas}[b] (%)	9.7 (106.2)	6.0 (140.6)	8.1 (91.5)	7.1 (81.0)
$\langle I/\sigma(I)\rangle$	24.7 (2.0)	26.5 (2.1)	15.0 (1.9)	12.0 (2.0)
Refinement				
R_{free} reflections	1144	1183	1074	2342
No. of atoms (non-hydrogen)				
Protein	2094	2098	8007	7994
Ligands	6	11	66	9
Solvent	312	280	1315	1071
R_{work}/R_{free} (%)	11.1/14.0	11.9/15.6	11.6/15.6	12.5/16.5
Average *B*-factor (Å^2)	19.0	22.0	18.0	24.0
RMSD[c] from ideal geometry				
Bond lengths (Å)	0.020	0.019	0.020	0.021
Bond angles (degrees)	2.09	1.95	1.89	1.99
Ramachandran statistics (%)				
Favored	95.8	97.0	97.2	97.2
Allowed	3.4	3.0	2.7	2.6
Outliers	0.4	0	0	0.1
PDB[d] code	**5EQ7**	**5EQ8**	**5EQ9**	**5EQA**

[a] Low and high resolution data were collected in two separate passes.
[b] R_{meas}, redundancy-independent *R*-factor (85).
[c] RMSD, root mean square deviation.
[d] PDB, protein data bank.

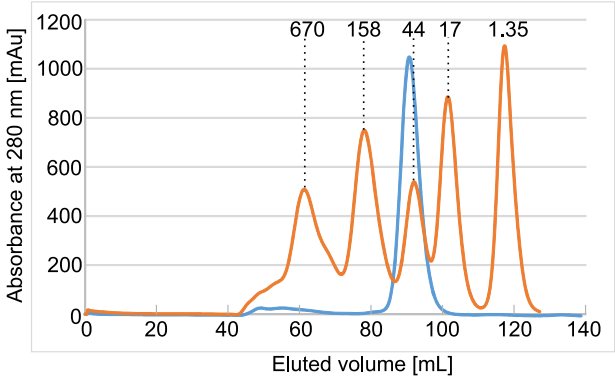

FIGURE 5. **Size exclusion chromatography of *Mt*HPP.** The standard is represented as a *red curve*, with molecular masses *above* each *peak* in kDa, whereas the *Mt*HPP elution profile is *blue*.

disordered in the presented structures. The eight-stranded β sheet of the N-terminal domain contains a ψ-loop motif (residues 131–149), where the β1 strand is flanked by strands β2 and β3. Moreover, a loop between strands β3 and β4 encompasses the helix α3. Strands β3–β8 have antiparallel organization. The linker between the N- and C-terminal domains consists of residues between Val^{202} and Asp^{209}. An extensive interface between the N- and C-terminal domains results in the rigidity of the entire structure, meaning that there is no hinge between the two domains, and they cannot move independently. The C-terminal domain, residues Leu^{210}–Trp^{326}, constitutes an $\alpha/\beta/\alpha$ fold, in which the mixed parallel/antiparallel β sheet is sandwiched between helices α6, η7 (3_{10} helix), and α8 from one side (close to the β sheet of the N-terminal domain) and η4, α5, and α9 from the other.

MtHPP Dimeric Assembly Is Stabilized by Intermolecular Lys-CH_2-Cys Covalent Bonds—Based on size exclusion chromatography, *Mt*HPP as well as mutants *Mt*HPP-T151A and *Mt*HPP-AAA are dimeric in solution, because they elute between the standard molecular mass markers of 158 and 44 kDa, significantly closer to the latter (Fig. 5). The PISA server (55) also suggests stable dimers, based on the monomer-monomer interfaces in the crystal structure. In the tetragonal crystal form (space group $P\,42_12$), with one protein molecule in the asymmetric unit, monomers in the dimer are related to each other by a crystallographic 2-fold axis with the symmetry operation $y, x, -z$. In the monoclinic crystal form ($P\,2_1$), where four protein subunits make up the asymmetric unit, two dimers are present (chains A + B and C + D), but the monomer-monomer interfaces are the same as in the tetragonal crystals. The buried surface area upon the dimer formation equals 3470 $Å^2$, whereas the surfaces of monomer and dimer equal 11,975 and 20,480 $Å^2$, respectively.

In the crystal structures of *Mt*HPP, a fascinating cross-linking interaction is observed within the dimer. Namely, methylene groups are present between Nζ atoms of Lys^{158} and Sγ atoms of Cys^{245}. This way, the dimer is stabilized by two methylene bridges as they form in a mutual and interchangeable manner (*i.e.* Lys^{158} from one protein subunit is linked to Cys^{245} of the other, and the binding also occurs the other way around) (Fig. 6*A*). In the presented *Mt*HPP complexes, the bond is observed at ~60% occupancy in the structures representing crystals that were harvested over 3 weeks after they had been grown (PO_4^{3-} and HOL complexes) but absent in crystal less than 2 weeks old (HOLP complex). Interestingly, this covalent dimerization could also be observed in protein solution that was kept in a CO_2 atmosphere where, after 20 days, dimers represent a substantial band on SDS-PAGE (Fig. 6*B*). It is also apparent that reducing agent prevents formation of covalent dimers, which, in the presence of TCEP, became barely observable after 20 days of the experiment, probably because a significant fraction of TCEP had degraded by that time.

Based on liquid chromatography-mass spectrometry (LC-MS) experiments, the relative abundance of dimers after 20 days in CO_2 atmosphere and in the absence of reducing agent was 17.4% (Fig. 6*C* and supplemental material S-3). The molecular mass of 61,358.75 Da is close to the calculated mass of 61,358.2 Da, corresponding to the doubled mass of the monomer, each with the N-terminal SNA linker that resides after cleavage with tobacco etch virus protease (2 × 30,378.3 Da), plus the difference from the two added methylene groups (24 Da) with SNAMSS adduct (577.6 Da) that most probably is an artifact resulting from the MS experiment.

The formation of methylene bridges most probably involves reaction of the primary amine of Lys^{158} with CO_2 to form carbamic acid (56). The carbon within the carbamic group possesses a partial positive charge, suitable for a nucleophilic attack by Sγ of Cys^{245} (57), but it is unclear how the cross-linking carbonyl is reduced to the methylene group. Theoretically, analogous bonds could form between any exposed cysteine and lysine residues, but they have never been reported. This suggests that the correct geometry (*i.e.* accurate location of Nζ and Sγ atoms of lysine and cysteine residues, respectively) must be ensured for the bond to form.

Moreover, when *Mt*HPP was subjected to formaldehyde, which is able to cross-link amines and thiols (58), the results were much more radical, although only HCHO vapors were allowed to contact the protein-containing solution in each case. More precisely, when the reservoir solution below the crystals was supplemented with 100 mM formaldehyde, the cross-linking was completed overnight by HCHO vapors diffusing into the crystallization drop (Fig. 6*A*). Consistently, the protein sample kept in an open vial placed in a closed bottle with formaldehyde at the bottom showed a high fraction of dimers after a 1-day incubation (Fig. 6, *B* and *C*). Inhomogeneity of monomers and dimers, observed on SDS-PAGE and MS, can be attributed to the fact that formaldehyde is a very potent agent in terms of reacting with proteins. Hence, *Mt*HPP was modified at multiple sites, which caused relatively wide distribution of molecular masses. Nonetheless, the presence of covalent dimers is clear using both methods for verification.

It is also of note that although neither Lys^{158} nor Cys^{245} takes part in the enzymatic reaction (see below), both residues are conserved in the *Arabidopsis* enzyme, which suggests that analogous cross-linking might occur also in *At*IMPL2. At this point, we are not able to unambiguously determine how the covalent dimerization influences the enzymatic reaction due to difficulties in obtaining a protein sample containing only covalent dimers. It would be of great interest to investigate the *in vivo* half-life of *Mt*HPP and correlate it with the time required to the

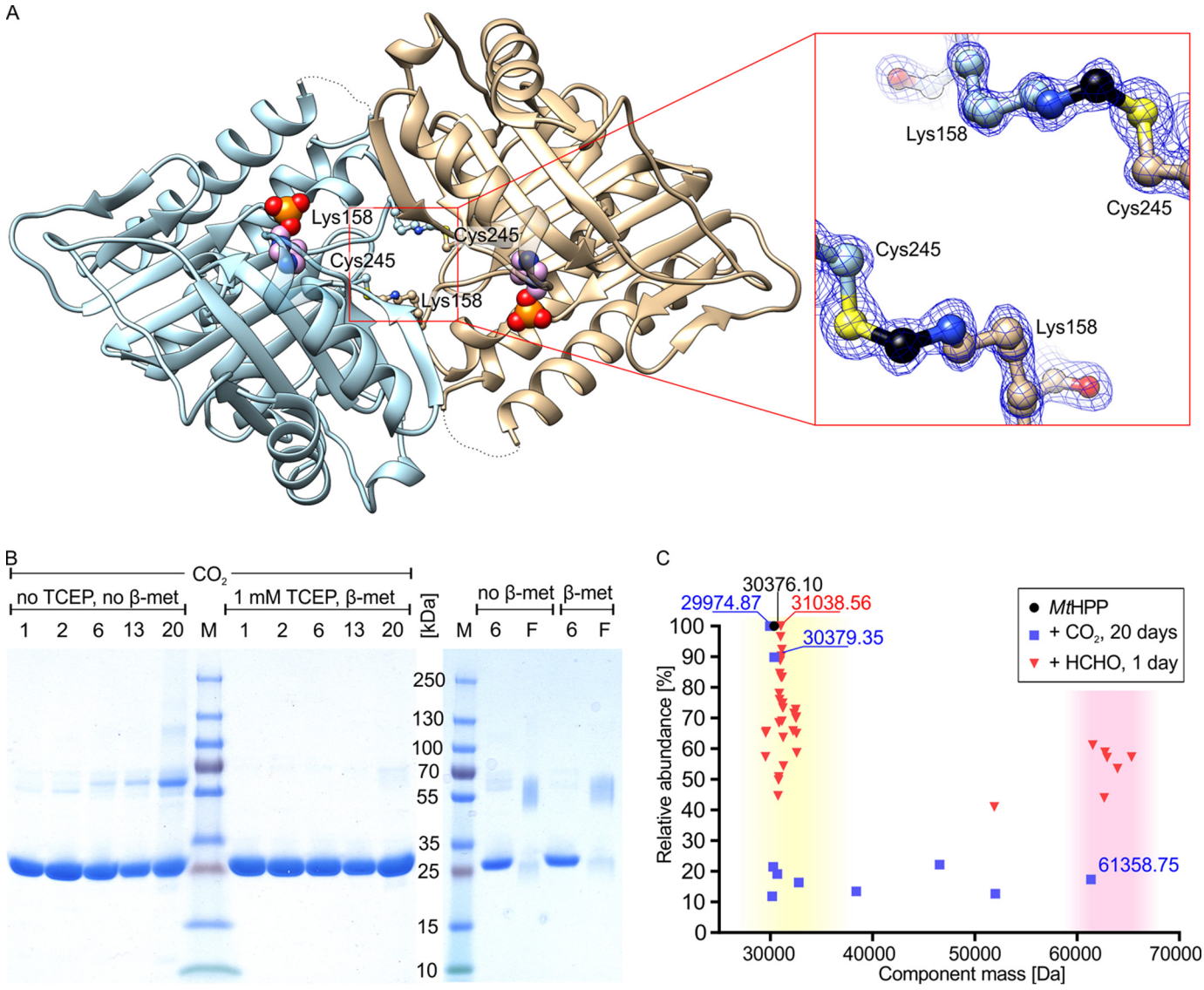

FIGURE 6. **Covalent dimerization of *Mt*HPP.** Chains A and B from the cross-linked *Mt*HPP structure, with superposed HOLP (*spheres*) from *Mt*HPP-HOLP complex, are presented in *A*. Residues 220–228 are *semitransparent* so that they do not obscure HOLP (*spheres*). The cross-linking Lys^{158} and Cys^{245} are shown as *ball-and-stick models*. The *close-up* on the *right* presents only the methylene-bridged (*black ball*) pairs of Lys^{158} and Cys^{245} contoured with a $2F_o - F_c$ electron density map (*Mt*HPP/Lys-CH_2-Cys structure) at 2 σ level shown as *blue mesh*. *B*, SDS-PAGE of MtHPP subjected to CO_2 atmosphere over 20 days (*left*) or formaldehyde (*F*) vapors for 24 h (*right*). *C*, summary of LC-MS experiments on fresh *Mt*HPP, cross-linked with CO_2 (non-reducing conditions) and formaldehyde (reducing conditions). Monomers and dimers are *highlighted* in *light yellow* and *pink*, respectively. See the supplemental material for detailed data.

Lys^{158}-CH_2-Cys^{245} bond to form. Unfortunately, whether it is a post-translational modification, a formaldehyde scavenging mechanism, or simply an artifact remains unclear. Nevertheless, both agents, CO_2 and formaldehyde, occur in each living cell, so it is likely that at least a small fraction of *Mt*HPP (or *At*IMPL2) could exist as covalent dimers *in vivo*.

HOLP Dephosphorylation Reaction Occurs at the Interface between N- and C-terminal Domains—Crystal structures of *Mt*HPP complexes obtained by swift (*Mt*HPP-HOLP complex) or prolonged (*Mt*HPP-HOL) soaking with the substrate (HOLP) or cocrystallization with by-product (PO_4^{3-}) provide very detailed information about the reaction catalyzed by the enzyme. From the *Mt*HPP complex with HOLP, we learn that the substrate is anchored to the protein by an extensive network of hydrogen bonds (Fig. 7*A*). Many of these bonds are mediated by water molecules that have low atomic displacement parameters. Namely, the Nϵ atom of HOLP via a water molecule interacts with the amide nitrogen atom of Ser^{264}, with a carbonyl oxygen of Leu^{222}, and, through another water, with Thr^{217} and Ser^{219}. Nδ forms a water-bridged hydrogen bond with a carbonyl oxygen of Gly^{265}. The N atom of HOLP forms direct hydrogen bonds with carboxyl oxygen atoms of Asp^{149} and Asp^{246} and a water-bridged interaction with carboxyl oxygen of Glu^{263}. The O atom of HOLP, where the hydrolysis occurs, interacts with the Asp^{246} by a water molecule, but this bond is weak, because the distance between HOLP O atom and the water molecule is >3.1 Å. The phosphate moiety interacts with amide nitrogen of Gly^{150}, Thr^{151} (OP1 atom of phosphate), and Oγ of Thr^{151} (OP2). The overall dipole moment of the α3 helix, of which Thr^{151} is the N-terminal residue, increases *Mt*HPP interaction with the phosphate moiety of HOLP. In addition, two lysines at positions 152 and 267, conserved in *At*IMPL2,

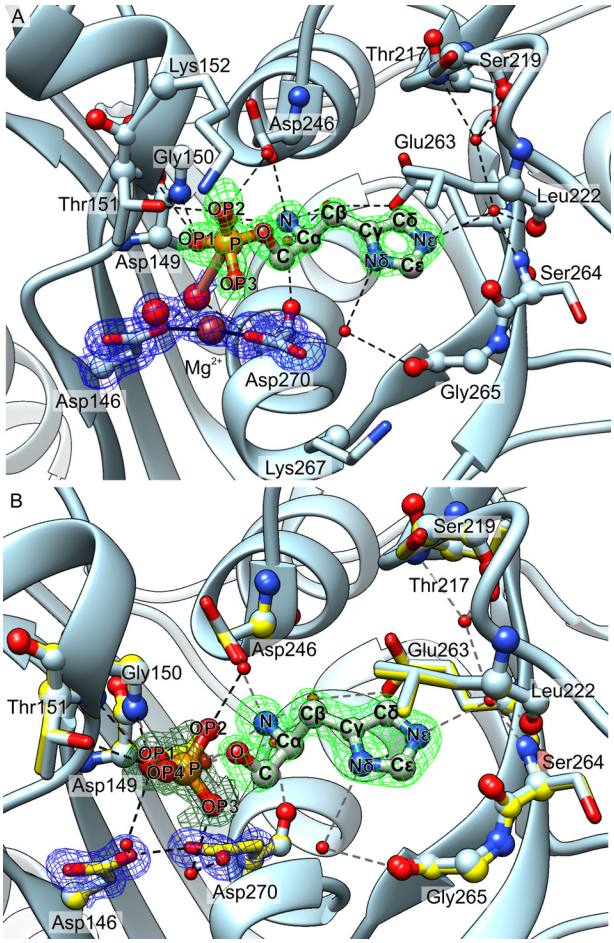

FIGURE 7. **The catalytic center of *Mt*HPP.** Binding of the substrate (HOLP) and Mg^{2+} from the HOLP-soaked crystal is shown in *A*, whereas interaction with product (HOL) and by-product (PO_4^{3-}), both resulting from cocrystallization, is presented in *B*. *Green mesh*, $F_o - F_c$ omit electron density map contoured around HOLP at 7 σ level (*A*), HOL at 4 σ (*B*), and PO_4^{3-} at 3 σ (*B*, *dark green*). *Blue mesh*, $2F_o - F_c$ map (at 1 σ) corresponding to side chains of Asp^{146}, Asp^{270}, Mg^{2+} (*brown ball*), and two conformations of the water molecule in the preactivated and activated state (*large red balls*) in *A*. The water in the activated state is linked to a phosphorus atom with a *stick* (*salmon*) for visualization purposes only. Other water molecules are shown as *red balls*. The *solid black lines* show ionic contacts of Mg^{2+}. In *B*, the protein chain from *Mt*HPP-PO_4^{3-} complex is *light blue*, and interacting residues from *Mt*HPP-HOL are *yellow*. The *large red ball* in *B* represents the positions of both the OP1 atom from the PO_4^{3-} complex and the water molecule that bridges the hydrogen bond between the oxygen atom of HOL and two peptide amides of Gly^{150} and Thr^{151}. *Black* and *gray dashed lines* indicate hydrogen bonds with PO_4^{3-} and HOL, respectively.

possibly act as claws that recruit HOLP (by its phosphate group) and guide the substrate at the initial phase of binding. A similar behavior of two Lys residues, surrounding the entrance to the active site, was proposed for NADP(H) binding to *M. truncatula* δ1-pyrroline-5-carboxylate reductase (59).

*Mt*HPP orients HOLP in such a way that the phosphate moiety is exposed to Asp^{146} and Asp^{270}. Those two aspartates coordinate a magnesium cation (at 0.7 occupancy) in the HOLP complex structure. The presence of Mg^{2+} cation was concluded based on O–Mg^{2+} distances that refined to 2.11 ± 0.07 Å (eight distances in four protein subunits were taken into account), which is very close to the ideal value of 2.107 (60). Those distances are certainly too short for a hydrogen bond involving a water molecule (≥2.4 Å), meaning that placement of a water molecule instead of Mg^{2+} would result in serious clashes. The Mg^{2+} cation separates Asp^{146} and Asp^{270} by 3.4 Å in the complex with HOLP. Without Mg^{2+} in between, as it is in all of the other *Mt*HPP structures presented, the conformation of the Asp^{270} side chain is different (Fig. 7), and the carboxyl groups of Asp^{146} and Asp^{270} directly interact with each other (shortest O–O distance is 2.4 Å). In that case, one of the carboxylic oxygen atoms of the aspartates (146 or 270) must be protonated and act as a hydrogen bond donor.

In the crystal structures of *Mt*HPP complexes, Mg^{2+} couples Asp^{146} and Asp^{270} only in the complex with HOLP, and we failed to incorporate the metal into any other complex, regardless of Mg^{2+} concentration tested (up to 20 mM). Also, in the absence of magnesium, we were unable to obtain *Mt*HPP complex with HOLP neither by cocrystallization nor by soaking. It is therefore likely that Mg^{2+} enters the active site complexed with HOLP, and both partners only bind together. There are, indeed, many negatively charged residues surrounding the active site that would repulse the negatively charged phosphate moiety of HOLP, and the substrate can only bind when complexed with Mg^{2+}, with a neutral net charge. Furthermore, it appears that after the hydrolysis has completed, Mg^{2+} leaves the active center, because in the structure obtained by 8-min soaking in HOLP, the product, HOL, was found in the cavity, but Mg^{2+} and PO_4^{3-} were not. The hypothesis that, in each reaction cycle, Mg^{2+} enters the active site with the substrate and leaves with free phosphate agrees with the fact that Mg^{2+} is bound to *Mt*HPP without a typical octahedral coordination sphere. The weakly bound Mg^{2+} can therefore easily escape the catalytic center. This observation is also consistent with the reported behavior of Mg^{2+} in human IMPase at a similar site, concluded to bind and dissociate as the catalysis proceeds (53, 61, 62).

Superposition of *Mt*HPP complexes with HOL and with PO_4^{3-} very well visualizes the immediate post-reaction state (Fig. 7*B*). One must remember, however, that this artificially constructed illustration still lacks Mg^{2+}. Protein chains from *Mt*HPP-PO_4^{3-} and HOL complexes superpose with a very small root mean square deviation of 0.1 Å (258 Cα pairs within a 3-Å radius). The free phosphate interacts in a manner very similar to that bound to HOLP. There are, however, two additional, water-mediated hydrogen bonds with Asp^{146} and Asp^{270} that, in this case, also directly interact with each other. HOL is bound nearly identically to HOLP, and the only difference is the hydrogen bond between the hydroxyl oxygen atom of HOL and two peptide amides of Gly^{150} and Thr^{151}, which is bridged by a water molecule that occupies the same location as OP1 in the HOLP or PO_4^{3-} complexes.

The fact that HOL is still present in the structure obtained by soaking *Mt*HPP crystals with HOLP, whereas Mg^{2+} and PO_4^{3-} are absent, might suggest a feedback inhibition mechanism. However, not only has it not been shown that HOL occurs *in vivo* at high concentration, but also HOL probably is rapidly converted to histidine by histidinol dehydrogenase. It is more likely that free His can suppress *Mt*HPP activity, but the His concentration in chloroplast is unknown (10). Nevertheless, it would be disadvantageous for a cell to produce HOLP already with high effort and halt at this point. Consistently, it has been elucidated that the pool of free His is controlled by ATP-phos-

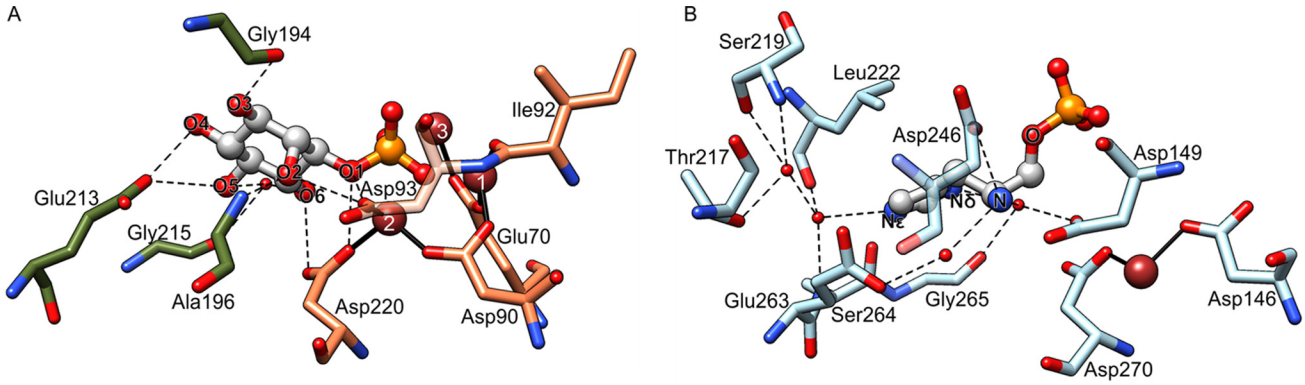

FIGURE 8. **Structural comparison of the active sites of IMPases and *Mt*HPP.** *A*, human IMPase (*Hs*IMPA1, *green* protein carbon atoms) in complex with IMP (*gray* carbon atoms; Protein Data Bank entry 1IMA (65)) with superposed Mg^{2+}-binding residues of bovine IMPase (*coral*, Protein Data Bank entry 2BJI (67)). *Numbering* of the shown residues is consistent between the bovine and human enzymes. *B*, *Mt*HPP-HOLP complex (*light blue* carbon atoms). Only the residues interacting with the substrates (except for the phosphate moieties) are shown in both *panels*.

phoribosyl transferase, the first enzyme in the His biosynthetic pathway (11, 63).

MtHPP and IMPases; Comparison of the Reaction Mechanism—The mechanism of reaction catalyzed by human IMPase was studied extensively in the last decade of the twentieth century due to an increasing amount of evidence indicating that human IMPase is a putative target of lithium therapy. Using numerous biochemical approaches, it was concluded that the hydrolysis of IMP involves a nucleophilic attack of a metal-activated water molecule (52, 53, 61, 62, 64–66). More precisely, two metal cations were proposed to bind within the active site and increase the nucleophilic character of a water molecule that directly attacks the phosphorus atom of the substrate. However, the structural positions of metal cations in the human IMPase were inferred from the complex with gadolinium cations (Gd^{3+}), which are significantly larger and are typically surrounded by more electron-donating ligands and, thus, do not ideally reflect Mg^{2+} binding sites. Finally, the structure of bovine IMPase, sharing 85% identity with the human enzyme, showed that even three Mg^{2+} cations may bind within the active site of bovine IMPase (67). To compare IMPases and *Mt*HPP, we superposed fragments of human IMPase (*Hs*IMPA1) in complex with IMP (Protein Data Bank entry 1IMA (65)) with Mg^{2+}-binding residues of bovine IMPase (Protein Data Bank entry 2BJI (67)) (Fig. 8). The three Mg^{2+} cations in bovine IMPase bind to the following (Fig. 8*A*; water-mediated interactions are excluded): site 1, carboxylic oxygen atoms of Glu^{70} (corresponding to Glu^{128} in *Mt*HPP) and Asp^{90} (Asp^{146}) and carbonyl of Ile^{92} (Ile^{148}); site 2, carboxylic oxygen atoms of Asp^{90} (Asp^{146}) and Asp^{220} (Asp^{270}); site 3, carboxyl of Glu^{70} (Glu^{128}). However, this structure was obtained in a 20 mM concentration of Mg^{2+}, which is outside the physiologically relevant range. It is therefore very likely that only Mg^{2+} binding site 1 with $K_d \approx 300$ μM (68) and site 2 with $K_d \approx 3$ mM (69) are occupied *in vivo*. More importantly, Mg^{2+} bound at site 1 was reported to remain tethered throughout the entire catalytic cycle, unlike Mg^{2+} at site 2 that binds and dissociates over the course of the reaction (53, 61, 62).

The crystal structures of *Mt*HPP complexes are consistent with the direct displacement of phosphate mechanism, reported for IMPases (70). Although, theoretically, Thr^{151} in *Mt*HPP could bear the phosphate and form a phosphoenzyme intermediate, it is very unlikely that this residue alone, without any metal cation, could perform a nucleophilic attack via a mechanism known for serine/threonine phosphatases (71). The residue structurally corresponding to Thr^{151}, Thr^{95} of human IMPase, was excluded as the nucleophile, when the T95A mutant was shown to sustain partial activity (62). When the *Mt*HPP-T151A mutant, which did not show any detectable HPP activity, was cocrystallized with HOLP, the active site did not contain HOLP nor HOL (not shown). This suggests that in *Mt*HPP, Thr^{151} is probably required for efficient binding of the phosphate moiety of HOLP.

*Mt*HPP is an IMPase-like enzyme, although important modifications in the reaction mechanism can be inferred from *Mt*HPP structures. At this point, it is noteworthy that the structures presented herein were derived from enzymatically active crystals. The most significant difference is the lack of Mg^{2+} cation at binding site 1 of bovine IMPase in any of the *Mt*HPP complexes and binding of Mg^{2+} at a location similar to site 2 in *Mt*HPP-HOLP complex (Fig. 8). The role of Mg^{2+} cations at sites 1 and 2 has been puzzling, because initially, it was reported that in bovine IMPase, Mg^{2+} at site 1 interacted with the phosphate, but Mg^{2+} at site 2 was proposed to be responsible for activation of the water molecule (72–74). In that scenario, the nucleophilic attack would start from the site adjacent to the leaving group (HOL) and proceed in a non-inline pathway with pseudorotation, which means that the configuration of the phosphorus atom would be retained. Later, for the same enzyme, using [^{16}O,^{17}O,^{18}O]thiophosphate substrate analogue, it was shown that it is actually the opposite (*i.e.* action of bovine IMPase results in the inversion of phosphate configuration, and it is Mg^{2+}-1 that activates water) (75, 76). This contrasts with the case of *Mt*HPP, which does not bind Mg^{2+} at the position corresponding to site 1 in bovine IMPase. When Mg^{2+} is bound to *Mt*HPP, the metal separates Asp^{146} and Asp^{270}, and negative charge of those aspartates is neutralized. However, in bovine IMPase, the Mg^{2+}-2 cation is bound ahead of the two aspartates (Asp^{90} and Asp^{220}), whereas Asp^{146} and Asp^{270} at the corresponding structural positions in *Mt*HPP coordinate the metal behind the two carboxylic groups (Fig. 8). Obviously, in *Mt*HPP, the Mg^{2+}-harnessed pair of Asp^{146} and Asp^{270} may

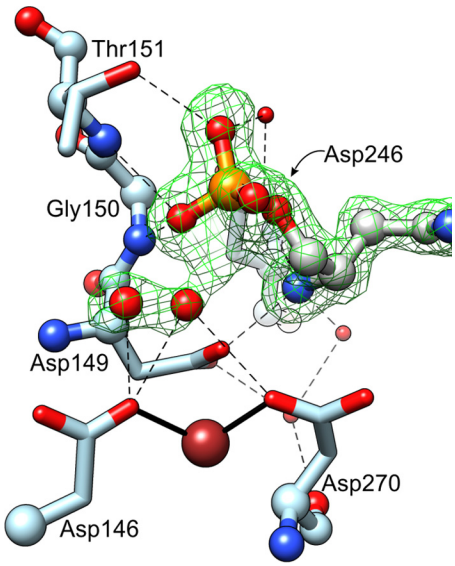

FIGURE 9. **Non-inline nucleophilic attack.** The water molecule (two states, *large red balls*) is activated by Asp^{146} and Asp^{270}, which bind Mg^{2+} (*brown ball*). *Green mesh*, omit $F_o - F_c$ electron density map contoured at 4.5 σ.

still attract hydrogen of the water molecule, thus providing an active nucleophilic agent, but the water molecule is activated indirectly, by magnesium-bound aspartates, and not directly by aspartate-bound metal, as in bovine IMPase (67). It must be noted that the hydrolysis catalyzed by *Mt*HPP needs to be performed by a water molecule and not by a hydroxyl anion, because the latter would be repulsed by likewise negatively charged phosphate. In the crystal structure of *Mt*HPP-HOLP complex, this "attacking" water molecule is observed at two alternative locations (Figs. 7*A* and 9), most probably one of which represents the state before activation and the other after activation. Water molecule at the position representing the preactivated state is present in other *Mt*HPP complexes at full occupancy. In *Mt*HPP-HOLP complex, the distance between the activated water and the phosphorus atom of HOLP is 3.1 Å, which is expected for a direct nucleophilic attack. The electron density for the active H_2O is in fact uninterrupted between the two alternative conformations (preactivated and activated state), separated by ~1.7 Å, but then it narrows and continues toward the phosphorus atom of HOLP (Fig. 9), meaning that even more transient states are captured within the crystal (*i.e.* averaged in the presented electron density maps). The shape of the electron density maps for HOLP and the attacking water molecule (Fig. 9) clearly indicates that the nucleophile attacks from the same face of the phosphorus atom as the leaving group (HOL). In other words, MtHPP catalyzes the reaction that proceeds in a non-inline pathway. The course of the non-inline reaction has been established using non-enzymatic systems (77). It was shown that the intermediate pentacovalent phosphate (78) undergoes a pseudorotation, because the initially apical nucleophile moves to an equatorial position, whereas the leaving group moves from an equatorial to apical orientation. This results in retention of the configuration of phosphorus.

In the last step of the reaction, the oxyanion oxygen atom that remains at HOL after the hydrolysis retrieves the proton from the oxygen of the water molecule that performs the attack and becomes a part of free phosphate or from a different H_2O/H_3O^+ or from the amino group of HOLP. There are no other potential proton donors, because the carboxyl oxygen atoms of Asp^{149} and Asp^{246}, although they are within a 4-Å radius, still coordinate amine nitrogen of HOLP and thus must be deprotonated.

Elements of the C-terminal Domain Are Responsible for Specificity toward HOLP—The sequence alignment (Fig. 2) indicates that the N-terminal domains of IMPases and IMPase-like HPPs are more conserved than their C-terminal domains. In fact, identities shared by *Mt*HPP and *At*IMPL1 equal 25% for the N-terminal and 16% for the C-terminal domains. As shown above, the residues that interact with the phosphate (Asp^{149}, Gly^{150}, and Thr^{151}) belong to the N-terminal domain. So does Asp^{146}, which coordinates Mg^{2+} and, according to the mechanism proposed in this paper, activates a water molecule that performs the nucleophilic attack. Therefore, Asp^{270} is the only residue directly involved in the enzymatic reaction that resides in the C-terminal domain. Simultaneously, Asp^{270} is one of a few C-terminal residues conserved among proteins from the IMPase family.

The crystal structure of *Mt*HPP-HOLP complex shows that binding of the HOL moiety of substrate involves many residues from the C-terminal domain (Thr^{217}, Ser^{219}, Leu^{222}, Asp^{246}, Glu^{263}, Ser^{264}, Gly^{265}, and Asp^{270}) and the side chain of Asp^{149} (N-terminal domain). The comparison of active sites (Fig. 8) gives a clear vista on many differences between IMP binding by IMPases and HOLP binding by *Mt*HPP, although some substrate-interacting residues are universal (*e.g.* Gly^{265} in *Mt*HPP and Gly^{215} in *Hs*IMPA1; Glu^{263}/Glu^{213}). The most important modification that enables *Mt*HPP to bind HOLP is the presence of Asp^{246}, which, by its carboxyl oxygen atom, forms a hydrogen bond with N atom of HOLP. The O2 atom of IMP, which lies in a similar location, is bound to *Hs*IMPA1 by the backbone amide of Ala^{196}. This alanine residue is conserved in other IMPases (*e.g.* Ala^{275} in *At*IMPL1; Fig. 2) that do not catalyze hydrolysis of HOLP. It is likely that the amide exposed to the catalytic pocket prevents HOLP from entering to an active site of IMPase because it would result in disfavored amide-amine interaction. Asp^{246} of *Mt*HPP is conserved not only in *At*IMPL2 but also in prokaryotic IMPase-like HPPs, CghisN and SchisN (24, 25), which allows us to postulate that the aspartate corresponding to position 246 in *Mt*HPP sequence is required for binding of HOLP. Consistently, the *Mt*HPP-AAA mutant, in which the genuine ^{245}CDC^{247} fragment was substituted with ^{245}AAA^{247} (as in *At*IMPL1), was unable to catalyze HOLP to HOL hydrolysis. On the other hand, the *Mt*HPP-AAA mutant remained inactive against IMP (as wild-type *Mt*HPP), which suggests that the substrate recognition is more complex.

The analysis of amino acid sequences of IMPase-like HPPs and IMPases (Fig. 2) indicates another element that differs between the two protein families. According to PROSITE (79), IMPases contain two consensus patterns: (F/W/V)$X_{0,1}$(L/I/V/M)DP(L/I/V/M)D(S/G)(S/T)X_2(F/Y/A)$X_{0,1}$(H/K/R/N/S/T/Y) (ID: PS00629) within the N-terminal domain and (W/Y/V)DX(A/C)(G/S/A)(G/S/A/P/V)X(L/I/V/F/A/C/P)(L/I/V/M)(L/I/V/A/C)X_3(G/H)(G/A) (PS00630) within the C-terminal domain (Fig. 2). All four so far confirmed IMPase-like HPPs,

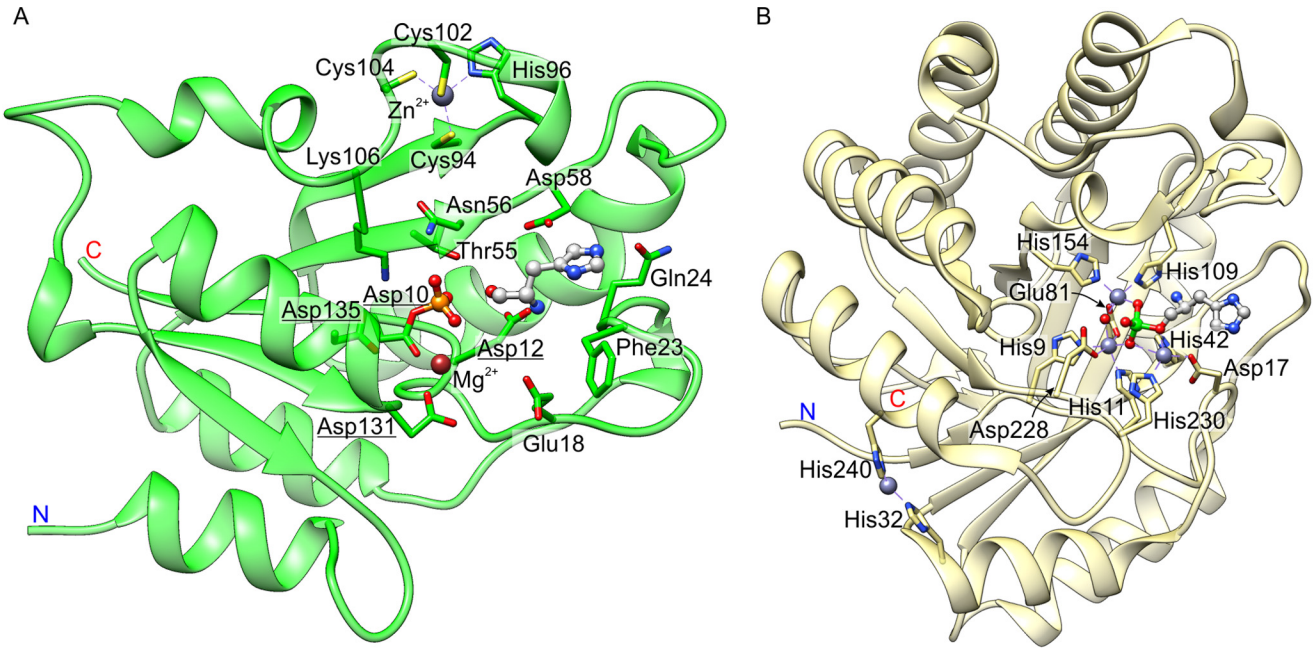

FIGURE 10. **Examples of HPP proteins from DDDD and PHP superfamilies.** *A*, the protein chain of *E. coli* HisB-N phosphoaspartate complex (Protein Data Bank entry 2FPW) is shown with superposed HOL (*gray* carbon atoms, *ball-and-stick model*) and Mg^{2+} from Protein Data Bank entry 2FPU structure (83). The four conserved Asp residues that give the DDDD superfamily its name are *underlined*. *B*, *Ll*HPP, from the PHP superfamily, in complex with L-histidinol-arsenate (*gray* carbon atoms, *ball-and-stick model*, 4GK8 (84)). *Magenta spheres*, locations of Zn^{2+} cations.

including *Mt*HPP, lack the PS00630 pattern but contain the N-terminal PS00629 pattern. Both observations, the presence of the Asp residue at a position corresponding to 246 in MtHPP and the lack of the C-terminal consensus pattern, sketch the route for future determination of more IMPase-like HPP enzymes.

MtHPP Bears No Resemblance to HPP Enzymes from DDDD or PHP Families—As mentioned in the Introduction, in nature there exist two other superfamilies of enzymes that catalyze dephosphorylation of HOLP to produce HOL, apart from the IMPase-like HPPs. Members of one of those two other HPP superfamilies are haloacid dehalogenase-like enzymes (80). They contain four invariant aspartate residues; hence the name of the superfamily, DDDD (21). In *E. coli* and in other protobacteria, DDDD domains responsible for HPP activity are a part of larger and bifunctional proteins, whose N-terminal domains possess HPP activities, whereas C-terminal domains are imidazole glycerol phosphate dehydratases (81). In *E. coli* HPP enzyme, the N-terminal domain of HisB (HisB-N), with a molecular mass of 19.9 kDa, is an about one-third smaller enzyme than *Mt*HPP. Although HisB-N also uses aspartate residues for anchoring the Mg^{2+} cation (Asp^{10} and Asp^{131}), the arrangement of the active site and the protein fold (Fig. 10) are completely different from that of *Mt*HPP. DDDD enzymes utilize a single metal cation (usually Mg^{2+}) to catalyze dephosphorylation, but the reaction proceeds via an aspartyl-phosphate intermediate (82). This covalent enzyme-phosphate adduct has even been captured in a crystal structure of HisB-N (83). A second reaction step, nucleophilic attack of a water molecule, is required to release the phosphate group from Asp and recycle the enzyme. The entire process involves double inversion of configuration of the phosphorus atom (*i.e.* overall, the configuration is retained).

*Mt*HPP, the IMPase-like HPP, executes a single-step reaction, in which the non-inline nucleophilic attack is performed by an activated water molecule (see above). In *Mt*HPP, the Mg^{2+}-tethering Asp^{146} and Asp^{270} are too distant from the phosphorus atom (>5 Å), which excludes the possibility of Asp-phosphate covalent complex formation. In the case of *Mt*HPP, the retention of the conformation of the phosphorus atom results from pseudorotation and not from double inversion as in HPPs from the DDDD superfamily. The differences in reaction mechanism are reflected by the very diverse turnover rates of IMPase-like and DDDD HPPs. The k_{cat} value for *Mt*HPP is 3.6 s^{-1}, whereas HisB-N converts HOLP to HOL nearly 3 orders of magnitude faster, with $k_{cat} = 2.14 \times 10^3$ s^{-1} (83). HisB-N also has a ~5 times lower K_m (54 μM) than does *Mt*HPP, making the latter, and all other examples of IMPase-like HPPs, relatively inefficient enzymes.

Some prokaryotes rely on HPP enzymes from the PHP superfamily. One such example is *Lactococcus lactis* HPP (*Ll*HPP). *Ll*HPP protein is folded into a distorted $(\beta/\alpha)_7$ barrel and possesses a trinuclear metal center (usually three Zn^{2+}) within the active site (84). Two of those metal ions coordinate a hydroxide ion, which functions as the hydrolytic nucleophile. The third Zn^{2+} coordinates the oxygen atom of HOLP, where the hydrolysis occurs. In *Ll*HPP, the three metal cations in the active center are coordinated by six His side chains, two Asp and one Glu (Fig. 10*B*). The fourth Zn^{2+} is bound outside the catalytic center and does not play a role in the enzymatic reaction. *Ll*HPP is slower than *E. coli* HisB-N from the DDDD superfamily and turns over with $k_{cat} = 174$ s^{-1}, still nearly 50 times faster than *Mt*HPP does. On the other hand, *Ll*HPP is characterized by a relatively high $K_m = 1.9$ mM.

The studies of *Mt*HPP presented here show that it is completely unrelated to either of the two other HPP superfamilies,

DDDD or PHP. *Mt*HPP, as an example of IMPase-like, plant HPPs, is significantly less efficient than examples from the other two superfamilies. This raises the question of what caused this evolutionary curiosity of three unrelated housekeeping enzymes. So far, it appears that there are not many examples of confirmed IMPase-like HPPs; therefore, a thorough evolutionary analysis is difficult. The structural and functional studies of *Mt*HPP presented here give hints to distinguish IMPase-like HPPs from IMPases, which facilitate separation of the two types of enzymes. With more metagenomic data, it should soon be possible to trace the evolutionary origin of plant HPPs.

Author Contributions—M. R. designed and performed the studies, analyzed the results, and wrote the manuscript. Z. D. analyzed the results and supervised the work.

Acknowledgments—We gratefully acknowledge Dr. Joanna Banasiak for assistance with identification of the MTHPP gene. We are also thankful to Dr. Jerry Alexandratos, who performed LC-MS studies at the Biophysics Resource in the Structural Biophysics Laboratory, National Cancer Institute at Frederick. Diffraction data were collected at the (i) SER-CAT beamline 22-ID at the Advanced Photon Source, Argonne National Laboratory, supported by the United States Department of Energy, Office of Science, Office of Basic Energy Sciences under Contract W-31-109-Eng-38 and (ii) Structural Biology Center at the Advanced Photon Source, operated by UChicago Argonne, LLC, for the United States Department of Energy, Office of Biological and Environmental Research under Contract DE-AC02-06CH11357.

References

1. Eicher, T., Hauptmann, S., and Speicher, A. (2003) *The Chemistry of Heterocycles: Structure, Reactions, Syntheses, and Applications*, 2nd Ed., John Wiley & Sons, Inc., New York
2. Kramer, U., CotterHowells, J. D., Charnock, J. M., Baker, A. J. M., and Smith, J. A. C. (1996) Free histidine as a metal chelator in plants that accumulate nickel. *Nature* **379,** 635–638
3. Ingle, R. A., Mugford, S. T., Rees, J. D., Campbell, M. M., and Smith, J. A. (2005) Constitutively high expression of the histidine biosynthetic pathway contributes to nickel tolerance in hyperaccumulator plants. *Plant Cell* **17,** 2089–2106
4. West, A. H., and Stock, A. M. (2001) Histidine kinases and response regulator proteins in two-component signaling systems. *Trends Biochem. Sci.* **26,** 369–376
5. Young, V. R. (1994) Adult amino acid requirements: the case for a major revision in current recommendations. *J. Nutr.* **124,** 1517S–1523S
6. Seligmann, H. (2003) Cost-minimization of amino acid usage. *J. Mol. Evol.* **56,** 151–161
7. Alifano, P., Fani, R., Liò, P., Lazcano, A., Bazzicalupo, M., Carlomagno, M. S., and Bruni, C. B. (1996) Histidine biosynthetic pathway and genes: structure, regulation, and evolution. *Microbiol. Rev.* **60,** 44–69
8. Akashi, H., and Gojobori, T. (2002) Metabolic efficiency and amino acid composition in the proteomes of *Escherichia coli* and *Bacillus subtilis*. *Proc. Natl. Acad. Sci. U.S.A.* **99,** 3695–3700
9. Swire, J. (2007) Selection on synthesis cost affects interprotein amino acid usage in all three domains of life. *J. Mol. Evol.* **64,** 558–571
10. Ingle, R. A. (2011) Histidine biosynthesis. *Arabidopsis Book* **9,** e0141
11. Koslowsky, S., Riegler, H., Bergmüller, E., and Zrenner, R. (2008) Higher biomass accumulation by increasing phosphoribosylpyrophosphate synthetase activity in *Arabidopsis thaliana* and *Nicotiana tabacum*. *Plant Biotechnol. J.* **6,** 281–294
12. Stepansky, A., and Leustek, T. (2006) Histidine biosynthesis in plants. *Amino Acids* **30,** 127–142
13. Wiater, A., Krajewska-Grynkiewicz, K., and Klopotowski, T. (1971) Histidine biosynthesis and its regulation in higher plants. *Acta Biochim. Pol.* **18,** 299–307
14. Fujimori, K., and Ohta, D. (1998) Isolation and characterization of a histidine biosynthetic gene in *Arabidopsis* encoding a polypeptide with two separate domains for phosphoribosyl-ATP pyrophosphohydrolase and phosphoribosyl-AMP cyclohydrolase. *Plant Physiol.* **118,** 275–283
15. Fujimori, K., Tada, S., Kanai, S., and Ohta, D. (1998) Molecular cloning and characterization of the gene encoding *N*′-[(5′-phosphoribosyl)-formimino]-5-aminoimidazole-4-carboxamide ribonucleotide (BBM II) isomerase from *Arabidopsis thaliana*. *Mol. Gen. Genet.* **259,** 216–223
16. Fujimori, K., and Ohta, D. (1998) An *Arabidopsis* cDNA encoding a bifunctional glutamine amidotransferase/cyclase suppresses the histidine auxotrophy of a *Saccharomyces cerevisiae* his7 mutant. *FEBS Lett.* **428,** 229–234
17. El Malki, F., Frankard, V., and Jacobs, M. (1998) Molecular cloning and expression of a cDNA sequence encoding histidinol phosphate aminotransferase from *Nicotiana tabacum*. *Plant Mol. Biol.* **37,** 1013–1022
18. Wong, Y. S., and Mazelis, M. (1981) Detection and properties of L-histidinol dehydrogenase in wheat-germ. *Phytochemistry* **20,** 1831–1834
19. Nagai, A., Ward, E., Beck, J., Tada, S., Chang, J. Y., Scheidegger, A., and Ryals, J. (1991) Structural and functional conservation of histidinol dehydrogenase between plants and microbes. *Proc. Natl. Acad. Sci. U.S.A.* **88,** 4133–4137
20. Nagai, A., and Scheidegger, A. (1991) Purification and characterization of histidinol dehydrogenase from cabbage. *Arch. Biochem. Biophys.* **284,** 127–132
21. Thaller, M. C., Schippa, S., and Rossolini, G. M. (1998) Conserved sequence motifs among bacterial, eukaryotic, and archaeal phosphatases that define a new phosphohydrolase superfamily. *Protein Sci.* **7,** 1647–1652
22. Lee, H. S., Cho, Y., Lee, J. H., and Kang, S. G. (2008) Novel monofunctional histidinol-phosphate phosphatase of the DDDD superfamily of phosphohydrolases. *J. Bacteriol.* **190,** 2629–2632
23. le Coq, D., Fillinger, S., and Aymerich, S. (1999) Histidinol phosphate phosphatase, catalyzing the penultimate step of the histidine biosynthesis pathway, is encoded by ytvP (hisJ) in *Bacillus subtilis*. *J. Bacteriol.* **181,** 3277–3280
24. Mormann, S., Lömker, A., Rückert, C., Gaigalat, L., Tauch, A., Pühler, A., and Kalinowski, J. (2006) Random mutagenesis in *Corynebacterium glutamicum* ATCC 13032 using an IS6100-based transposon vector identified the last unknown gene in the histidine biosynthesis pathway. *BMC Genomics* **7,** 205
25. Marineo, S., Cusimano, M. G., Limauro, D., Coticchio, G., and Puglia, A. M. (2008) The histidinol phosphate phosphatase involved in histidine biosynthetic pathway is encoded by SCO5208 (hisN) in *Streptomyces coelicolor* A3(2). *Curr. Microbiol.* **56,** 6–13
26. Torabinejad, J., Donahue, J. L., Gunesekera, B. N., Allen-Daniels, M. J., and Gillaspy, G. E. (2009) VTC4 is a bifunctional enzyme that affects myoinositol and ascorbate biosynthesis in plants. *Plant Physiol.* **150,** 951–961
27. Petersen, L. N., Marineo, S., Mandalà, S., Davids, F., Sewell, B. T., and Ingle, R. A. (2010) The missing link in plant histidine biosynthesis: *Arabidopsis* myoinositol monophosphatase-like2 encodes a functional histidinol-phosphate phosphatase. *Plant Physiol.* **152,** 1186–1196
28. Nourbakhsh, A., Collakova, E., and Gillaspy, G. E. (2014) Characterization of the inositol monophosphatase gene family in *Arabidopsis*. *Front. Plant Sci.* **5,** 725
29. Kim, Y., Babnigg, G., Jedrzejczak, R., Eschenfeldt, W. H., Li, H., Maltseva, N., Hatzos-Skintges, C., Gu, M., Makowska-Grzyska, M., Wu, R., An, H., Chhor, G., and Joachimiak, A. (2011) High-throughput protein purification and quality assessment for crystallization. *Methods* **55,** 12–28
30. Klock, H. E., and Lesley, S. A. (2009) The polymerase incomplete primer extension (PIPE) method applied to high-throughput cloning and site-directed mutagenesis. *Methods Mol. Biol.* **498,** 91–103
31. Kabsch, W. (2010) XDS. *Acta Crystallogr. D Biol. Crystallogr.* **66,** 125–132
32. McCoy, A. J., Grosse-Kunstleve, R. W., Adams, P. D., Winn, M. D., Storoni, L. C., and Read, R. J. (2007) Phaser crystallographic software. *J. Appl. Crystallogr.* **40,** 658–674

33. Hwang, H. J., Park, S. Y., and Kim, J. S. (2014) Crystal structure of cbbF from *Zymomonas mobilis* and its functional implication. *Biochem. Biophys. Res. Commun.* **445,** 78–83
34. Langer, G., Cohen, S. X., Lamzin, V. S., and Perrakis, A. (2008) Automated macromolecular model building for x-ray crystallography using ARP/wARP version 7. *Nat. Protoc.* **3,** 1171–1179
35. Kowiel, M., Jaskolski, M., and Dauter, Z. (2014) ACHESYM: an algorithm and server for standardized placement of macromolecular models in the unit cell. *Acta Crystallogr. D Biol Crystallogr.* **70,** 3290–3298
36. Emsley, P., Lohkamp, B., Scott, W. G., and Cowtan, K. (2010) Features and development of Coot. *Acta Crystallogr. D Biol. Crystallogr.* **66,** 486–501
37. Murshudov, G. N., Skubák, P., Lebedev, A. A., Pannu, N. S., Steiner, R. A., Nicholls, R. A., Winn, M. D., Long, F., and Vagin, A. A. (2011) REFMAC5 for the refinement of macromolecular crystal structures. *Acta Crystallogr. D Biol. Crystallogr.* **67,** 355–367
38. Baykov, A. A., Evtushenko, O. A., and Avaeva, S. M. (1988) A malachite green procedure for orthophosphate determination and its use in alkaline phosphatase-based enzyme immunoassay. *Anal. Biochem.* **171,** 266–270
39. Pettersen, E. F., Goddard, T. D., Huang, C. C., Couch, G. S., Greenblatt, D. M., Meng, E. C., and Ferrin, T. E. (2004) UCSF Chimera: a visualization system for exploratory research and analysis. *J. Comput. Chem.* **25,** 1605–1612
40. Lovell, S. C., Davis, I. W., Arendall, W. B., 3rd, de Bakker, P. I., Word, J. M., Prisant, M. G., Richardson, J. S., and Richardson, D. C. (2003) Structure validation by C-α geometry: ϕ,ψ and C-β deviation. *Proteins* **50,** 437–450
41. Hutchinson, E. G., and Thornton, J. M. (1996) PROMOTIF: a program to identify and analyze structural motifs in proteins. *Protein Sci.* **5,** 212–220
42. de Beer, T. A., Berka, K., Thornton, J. M., and Laskowski, R. A. (2014) PDBsum additions. *Nucleic Acids Res.* **42,** D292–D296
43. Altschul, S. F., Madden, T. L., Schäffer, A. A., Zhang, J., Zhang, Z., Miller, W., and Lipman, D. J. (1997) Gapped BLAST and PSI-BLAST: a new generation of protein database search programs. *Nucleic Acids Res.* **25,** 3389–3402
44. Tamura, K., Stecher, G., Peterson, D., Filipski, A., and Kumar, S. (2013) MEGA6: Molecular Evolutionary Genetics Analysis version 6.0. *Mol. Biol. Evol.* **30,** 2725–2729
45. Emanuelsson, O., Nielsen, H., Brunak, S., and von Heijne, G. (2000) Predicting subcellular localization of proteins based on their N-terminal amino acid sequence. *J. Mol. Biol.* **300,** 1005–1016
46. Nielsen, H., Engelbrecht, J., Brunak, S., and von Heijne, G. (1997) Identification of prokaryotic and eukaryotic signal peptides and prediction of their cleavage sites. *Protein Eng.* **10,** 1–6
47. Altschul, S. F., Gish, W., Miller, W., Myers, E. W., and Lipman, D. J. (1990) Basic local alignment search tool. *J. Mol. Biol.* **215,** 403–410
48. Tang, H., Krishnakumar, V., Bidwell, S., Rosen, B., Chan, A., Zhou, S., Gentzbittel, L., Childs, K. L., Yandell, M., Gundlach, H., Mayer, K. F., Schwartz, D. C., and Town, C. D. (2014) An improved genome release (version Mt4.0) for the model legume *Medicago truncatula*. *BMC Genomics* **15,** 312
49. Ishijima, S., Uchibori, A., Takagi, H., Maki, R., and Ohnishi, M. (2003) Light-induced increase in free Mg^{2+} concentration in spinach chloroplasts: measurement of free Mg^{2+} by using a fluorescent probe and necessity of stromal alkalinization. *Arch. Biochem. Biophys.* **412,** 126–132
50. Heldt, W. H., Werdan, K., Milovancev, M., and Geller, G. (1973) Alkalization of the chloroplast stroma caused by light-dependent proton flux into the thylakoid space. *Biochim. Biophys. Acta* **314,** 224–241
51. Hauser, M., Eichelmann, H., Oja, V., Heber, U., and Laisk, A. (1995) Stimulation by light of rapid pH regulation in the chloroplast stroma *in vivo* as indicated by CO_2 solubilization in leaves. *Plant Physiol.* **108,** 1059–1066
52. Bone, R., Springer, J. P., and Atack, J. R. (1992) Structure of inositol monophosphatase, the putative target of lithium therapy. *Proc. Natl. Acad. Sci. U.S.A.* **89,** 10031–10035
53. Leech, A. P., Baker, G. R., Shute, J. K., Cohen, M. A., and Gani, D. (1993) Chemical and kinetic mechanism of the inositol monophosphatase reaction and its inhibition by Li^+. *Eur. J. Biochem.* **212,** 693–704
54. Hallcher, L. M., and Sherman, W. R. (1980) The effects of lithium ion and other agents on the activity of *myo*-inositol-1-phosphatase from bovine brain. *J. Biol. Chem.* **255,** 10896–10901
55. Krissinel, E., and Henrick, K. (2007) Inference of macromolecular assemblies from crystalline state. *J. Mol. Biol.* **372,** 774–797
56. Penny, D. E., and Ritter, T. J. (1983) Kinetic study of the reaction between carbon dioxide and primary amines. *J. Chem. Soc. Faraday Trans. I* **79,** 2103–2109
57. Włodek, L. (1988) The reaction of sulfhydryl groups with carbonyl compounds. *Acta Biochim. Pol.* **35,** 307–317
58. Metz, B., Kersten, G. F., Hoogerhout, P., Brugghe, H. F., Timmermans, H. A., de Jong, A., Meiring, H., ten Hove, J., Hennink, W. E., Crommelin, D. J., and Jiskoot, W. (2004) Identification of formaldehyde-induced modifications in proteins: reactions with model peptides. *J. Biol. Chem.* **279,** 6235–6243
59. Ruszkowski, M., Nocek, B., Forlani, G., and Dauter, Z. (2015) The structure of *Medicago truncatula* δ1-pyrroline-5-carboxylate reductase provides new insights into regulation of proline biosynthesis in plants. *Front. Plant Sci.* **6,** 869
60. Lang, P. F., and Smith, B. C. (2010) Ionic radii for Group 1 and Group 2 halide, hydride, fluoride, oxide, sulfide, selenide and telluride crystals. *J. Chem. Soc. Dalton Trans.* **39,** 7786–7791
61. Pollack, S. J., Atack, J. R., Knowles, M. R., McAllister, G., Ragan, C. I., Baker, R., Fletcher, S. R., Iversen, L. L., and Broughton, H. B. (1994) Mechanism of inositol monophosphatase, the putative target of lithium therapy. *Proc. Natl. Acad. Sci. U.S.A.* **91,** 5766–5770
62. Pollack, S. J., Knowles, M. R., Atack, J. R., Broughton, H. B., Ragan, C. I., Osborne, S., and McAllister, G. (1993) Probing the role of metal ions in the mechanism of inositol monophosphatase by site-directed mutagenesis. *Eur. J. Biochem.* **217,** 281–287
63. Rees, J. D., Ingle, R. A., and Smith, J. A. (2009) Relative contributions of nine genes in the pathway of histidine biosynthesis to the control of free histidine concentrations in *Arabidopsis thaliana*. *Plant Biotechnol. J.* **7,** 499–511
64. Bone, R., Frank, L., Springer, J. P., and Atack, J. R. (1994) Structural studies of metal binding by inositol monophosphatase: evidence for two-metal ion catalysis. *Biochemistry* **33,** 9468–9476
65. Bone, R., Frank, L., Springer, J. P., Pollack, S. J., Osborne, S. A., Atack, J. R., Knowles, M. R., McAllister, G., Ragan, C. I., and Broughton, H. B. (1994) Structural analysis of inositol monophosphatase complexes with substrates. *Biochemistry* **33,** 9460–9467
66. Saudek, V., Vincendon, P., Do, Q. T., Atkinson, R. A., Sklenar, V., Pelton, P. D., Piriou, F., and Ganzhorn, A. J. (1996) 7Li nuclear-magnetic-resonance study of lithium binding to *myo*-inositol monophosphatase. *Eur. J. Biochem.* **240,** 288–291
67. Gill, R., Mohammed, F., Badyal, R., Coates, L., Erskine, P., Thompson, D., Cooper, J., Gore, M., and Wood, S. (2005) High-resolution structure of *myo*-inositol monophosphatase, the putative target of lithium therapy. *Acta Crystallogr. D Biol. Crystallogr.* **61,** 545–555
68. Greasley, P. J., and Gore, M. G. (1993) Bovine inositol monophosphatase: studies on the binding interactions with magnesium, lithium and phosphate ions. *FEBS Lett.* **331,** 114–118
69. Greasley, P. J., Hunt, L. G., and Gore, M. G. (1994) Bovine inositol monophosphatase: ligand binding to pyrene-maleimide-labelled enzyme. *Eur. J. Biochem.* **222,** 453–460
70. Baker, G. R., and Gani, D. (1991) Inositol dependent phosphate-oxygen ligand-exchange catalyzed by inositol monophosphatase. *Bioorg. Med. Chem. Lett.* **1,** 193–196
71. Shi, Y. (2009) Serine/threonine phosphatases: mechanism through structure. *Cell* **139,** 468–484
72. Cole, A. G., and Gani, D. (1994) Active conformation of the inositol monophosphatase substrates adenosine 2′-phosphate and inositol phosphate: role of the ribofuranosyl O-atom and inositol O-atoms in chelating a 2nd magnesium ion. *J. Chem. Soc. Chem. Commun.* 1139–1141
73. Wilkie, J., Cole, A. G., and Gani, D. (1995) 3-Dimensional interactions between inositol monophosphatase and its substrates, inhibitors and metal-ion cofactors. *J. Chem. Soc. Perkin Trans.* **1,** 2709–2727
74. Wilkie, J., and Gani, D. (1996) Comparison of inline and non-inline associative and dissociative reaction pathways for model reactions of phosphate monoester hydrolysis. *J. Chem. Soc. Perkin Trans.* **2,** 783–787
75. Fauroux, C. M. J., Lee, M., Cullis, P. M., Douglas, K. T., Freeman, S., and

Gore, M. G. (1999) Inversion of configuration during the hydrolysis of D-1-*S*-*p*-*myo*-inositol [*O*-17]thiophosphate catalyzed by *myo*-inositol monophosphatase. *J. Am. Chem. Soc.* **121,** 8385–8386
76. Miller, D. J., Beaton, M. W., Wilkie, J., and Gani, D. (2000) The 6-OH group of D-inositol 1-phosphate serves as an H-bond donor in the catalytic hydrolysis of the phosphate ester by inositol monophosphatase. *Chembiochem* **1,** 262–271
77. Buchwald, S. L., Pliura, D. H., and Knowles, J. R. (1984) Stereochemical evidence for pseudorotation in the reaction of a phosphoric monoester. *J. Am. Chem. Soc.* **106,** 4916–4922
78. Lahiri, S. D., Zhang, G., Dunaway-Mariano, D., and Allen, K. N. (2003) The pentacovalent phosphorus intermediate of a phosphoryl transfer reaction. *Science* **299,** 2067–2071
79. Sigrist, C. J., de Castro, E., Cerutti, L., Cuche, B. A., Hulo, N., Bridge, A., Bougueleret, L., and Xenarios, I. (2013) New and continuing developments at PROSITE. *Nucleic Acids Res.* **41,** D344–D347
80. Aravind, L., Galperin, M. Y., and Koonin, E. V. (1998) The catalytic domain of the P-type ATPase has the haloacid dehalogenase fold. *Trends Biochem. Sci.* **23,** 127–129
81. Brilli, M., and Fani, R. (2004) Molecular evolution of hisB genes. *J. Mol. Evol.* **58,** 225–237
82. Allen, K. N., and Dunaway-Mariano, D. (2004) Phosphoryl group transfer: evolution of a catalytic scaffold. *Trends Biochem. Sci.* **29,** 495–503
83. Rangarajan, E. S., Proteau, A., Wagner, J., Hung, M. N., Matte, A., and Cygler, M. (2006) Structural snapshots of *Escherichia coli* histidinol phosphate phosphatase along the reaction pathway. *J. Biol. Chem.* **281,** 37930–37941
84. Ghodge, S. V., Fedorov, A. A., Fedorov, E. V., Hillerich, B., Seidel, R., Almo, S. C., and Raushel, F. M. (2013) Structural and mechanistic characterization of L-histidinol phosphate phosphatase from the polymerase and histidinol phosphatase family of proteins. *Biochemistry* **52,** 1101–1112
85. Diederichs, K., and Karplus, P. A. (1997) Improved R-factors for diffraction data analysis in macromolecular crystallography. *Nat. Struct. Biol.* **4,** 269–275